Power Monitoring Beyond Radial Distribution Networks

Brian T. Mills, Daisy H. Green, *Graduate Student Member, IEEE*, John S. Donnal, *Senior Member, IEEE*, and Steven B. Leeb, *Fellow, IEEE*

***Abstract*— Typical "last quarter mile" power distribution employs a radial network of electrical panels, feeders, and subpanels. Monitoring and fault localization on radial grids are relatively straightforward, as feeder connections to a panel provide a convenient single-access point for measuring current, voltage, and aggregate power. When multiple generating sources feed a local grid to provide redundancy or flexibility in the integration of diverse sources, a ring bus may be employed to power a mix of radial subnetworks. Monitoring individual loads from measurements made on a ring bus requires the combination of multiple measurements. These measurements must be precisely synchronized. In many cases, wireless time synchronization may be difficult to transmit, and wired time synchronization may be impractical to retrofit. In these scenarios, the power system itself can be used to align the data. This article introduces practical techniques to time-align measurements collected on a ring bus in order to monitor individual load power consumption. Marine microgrids are used to illustrate the presented time-alignment algorithms, and the results are demonstrated on ring-bus microgrid hardware.**

***Index Terms*— Microgrids, non-intrusive monitoring, power monitoring, ring bus, time synchronization.**

I. Introduction

In A radial power-distribution network, a source delivers power from the "root" of a collection of loads organized in a tree structure. Protection is relatively straightforward, typically based on calculation of available short circuit current calculated using line and system impedances. Load monitoring is also relatively easy: since power flows "out" from the source to a network of loads, one sensor on the "trunk" of the tree nonintrusively captures all power events.

Alternative distribution architectures are desirable in situations with diverse sources and a requirement for high-reliability, fault-tolerant operation. For example, the increase in distributed energy resources has increased the interest in dc ring microgrids, which provides increased reliability and efficiency by reducing power conversion stages [1]–[3]. Many naval vessels employ ring-bus distributions to provide redundancy and protection in the event of a failure [4]. Ring distribution loops the service from a source (or several different sources) through a collection of loads and back to the source. The ring can support ac or dc distribution and can combine sources with differing types and capacities. Interlocking rings can be separated or joined to form a larger network or microgrid with enhanced flexibility for interconnecting power. Since a ring bus can provide power in any direction on the ring or rings, a fault can be isolated while preserving services for vital loads. The variety of power transfer paths offers significant flexibility for maintenance, fault protection, and failure response.

Path multiplicity complicates automatic relaying or protection on a multiring system [5]–[8]. Therefore, complex monitoring systems may be necessary for mission-critical ring microgrids to measure ring voltages and currents in order to identify and isolate faults [7]. Unfortunately, this instrumentation does not naturally provide power consumption information for loads or systems, as the power provided to a load may arrive over multiple paths. Additional load monitoring hardware [such as a nonintrusive load monitor (NILM)] is typically installed on service panels at the root of radial networks fed by the ring [9].

These extra sensors for load monitoring should be unnecessary. With data from a fully instrumented ring bus, it is simple in principle to apply Kirchoff's current law (KCL) on the known grid architecture to determine the current flowing into radial distribution service panels further down the grid. However, the time alignment of each meter's data must be ensured to accurately reconstruct load power consumption. This is especially important for capturing load transients over hundredths or tenths of a second. Transient signatures serve as fingerprints that permit the recognition and disaggregation of load behavior. Power to a load delivered from multiple paths must be reconstructed from multiple measurements. Synchronization errors in data collection will distort transient shapes.

Clock synchronization is a challenging and heavily researched task for applications requiring meaningful sensor fusion, such as phasor measurement units (PMUs) [10]–[12]. Device-level time synchronization of PMUs typically relies on a reliable synchronizing signal, such as a clock derived from the global positioning system (GPS) [13]. In many smart meter applications, it is assumed that the measurements

Manuscript received September 12, 2021; revised November 28, 2021; accepted December 5, 2021. Date of publication December 14, 2021; date of current version March 2, 2022. This work was supported in part by the Grainger Foundation, in part by the Office of Naval Research Naval Enterprise Partnership Teaming with Universities for National Excellence (NEPTUNE) Program, and in part by Mathworks. The Associate Editor coordinating the review process was Datong Liu. *(Corresponding author: Daisy H. Green.)*

Brian T. Mills is with the United States Coast Guard, Washington, DC 20593 USA.

Daisy H. Green and Steven B. Leeb are with the Department of Electrical Engineering and Computer Science, Massachusetts Institute of Technology, Cambridge, MA 02139 USA (e-mail: dhgreen@mit.edu).

John S. Donnal is with the Department of Weapons, Robotics, and Control Engineering, United States Naval Academy, Annapolis, MD 21402 USA.

Digital Object Identifier 10.1109/TIM.2021.3135321

are synchronized. However, unlike PMUs, many smart meter measurements are not actually perfectly synchronized [14]. In practice, there may be significant time differences, which reduces the quality of the desired output [15]. Weak signal reception makes GPS and other wireless signals difficult to apply indoors [11]. For example, wireless synchronization solutions may be effectively impossible on small microgrids serving metal-hulled marine vessels [16], [17]. Synchronization is further complicated by drift due to temperature, electromagnetic interference (EMI), and vibration, all of which can affect the accuracy of digital clocks [12]. A wired and shared clock signal can synchronize different measurement systems, but this approach may be expensive to retrofit.

Reliable time alignment signals can be derived from the power system itself. This article explores a ring-bus microgrid similar to that found on many marine vessels. Techniques are developed for time-aligning and resolving the KCL sums in any part of the network. This "preprocessing" makes it possible to nonintrusively monitor collections of loads strictly from measurements made along the ring bus. That is, signals that are likely already available for protection and relaying on the ring can be used to monitor the grid loads in detail. Demonstrations of the proposed algorithms are presented on hardware.

II. Ring Bus: Shipboard Examples

The monitoring methods discussed in this article apply to any electrical distribution system with path multiplicity. Marine microgrids serve to illustrate our hardware and algorithms, but the approaches described here are applicable on any grid with path multiplicity. Ships use a variety of ring distribution systems to power vital loads, such as fire pumps, communications, and emergency lighting. For most commercial ships, simply having multiple generators can satisfy redundancy requirements, and system monitoring can be performed by meters on each generator. For military ships and certain commercial ships, such as dynamically positioned ships, interconnected switchboards are required to prevent loss of power from a failure.

On a naval vessel, the ring-bus distribution provides protection in the event of failures of entire switchboards or machinery rooms [4]. Vital loads are fed from two different switchboards via automatic bus transfers (ABTs). Because a switchboard or vital load can receive power through more than one path, power continuity and reliability are increased [18]. An example ring bus similar to that found on United States Coast Guard (USCG) National Security Cutters is shown in Fig. 1. Larger ring buses can be formed. For example, the Italian aircraft carrier Cavour uses eight circularly connected generators and switchboard installations [19].

The United States Navy uses an architecture called a zonal electric distribution system (ZEDS) on newer large ships, e.g., on destroyers (DDGs), amphibious transports, helicopter carriers, and aircraft carriers. The ZEDS, a series of interconnected rings, provides additional ability to isolate different elements during a fault [20], [21]. Zonal systems, such as the one shown in Fig. 2, typically use both a port and starboard bus running the length of the ship, with cross-ties at multiple points that

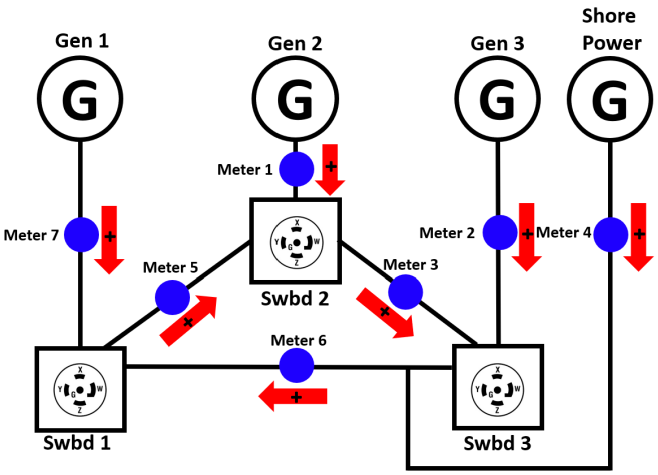

Fig. 1. Shipboard ring-bus example marked with monitoring locations.

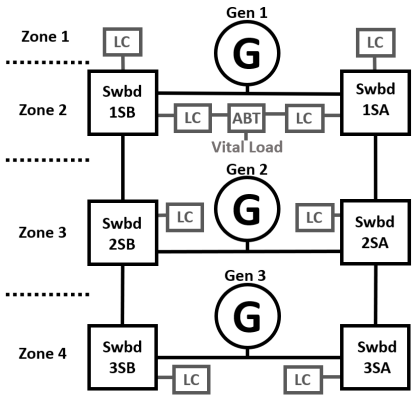

Fig. 2. Shipboard zonal electrical distribution system example.

form multiple rings. Each zone of the ship has at least one load center (LC) from each bus. The load center powers a radial subnetwork of loads.

Monitoring capabilities often already exist onboard ships for oversight of the ring distribution system but not necessarily for monitoring the status and health of individual pieces of equipment. Dual use could be made of the monitoring equipment already in place. For example, the ZEDS onboard United States Navy DDG-51s uses multifunction monitors (MFMs) for automated failure response. The MFMs observe the current and voltage at each switchboard bus tie and generator breaker, and communicate via a dedicated information network with each other to execute a coordinated shunt response to system faults [22], [23]. The voltage and current data collected by one MFM are translated to events or flags and are not used directly in calculations by any other MFM, thus avoiding time-alignment challenges [24]. Adding a time-alignment capability would allow MFM hardware, or other sensors already in place, to function as a load monitor.

For demonstration, a ring-bus distribution system was constructed for this article with a delta-configured bus. Each "meter," shown as blue circles in Fig. 1, consists of a data acquisition (DAQ) device fed by three LA-55 current sensors and three voltage connections, one for each phase. The DAQ samples current and voltage waveforms at 8 kHz and preprocesses the data to compute real power (P) and

reactive power (Q) at an output frequency equal to the system frequency of 60 Hz [25]. All seven DAQs communicate with a single computer that collates and time aligns this data to calculate power consumption for each switchboard.

With meters positioned to monitor all sources of power and all paths between switchboards, the power demand of each switchboard can be uniquely determined. Treating each switchboard as a "node," we construct the KCL matrix for the power system and sensor arrangement. Accounting for the polarity of the sensors shown in Fig. 1, a preprocessing matrix transforms measured ring-bus currents into switchboard currents and also total current provided by all of the generators to the ship. The monitoring system performs these calculations for each phase $\phi \in \{\text{A, B, C}\}$

$$\begin{bmatrix} I_{\text{swbd1},\phi} \\ I_{\text{swbd2},\phi} \\ I_{\text{swbd3},\phi} \\ I_{\text{ship},\phi} \end{bmatrix} = \begin{bmatrix} 0 & 0 & 0 & 0 & -1 & 1 & 1 \\ 1 & 0 & -1 & 0 & 1 & 0 & 0 \\ 0 & 1 & 1 & 1 & 0 & -1 & 0 \\ 1 & 1 & 0 & 1 & 0 & 0 & 1 \end{bmatrix} \begin{bmatrix} I_{\text{Meter1},\phi} \\ I_{\text{Meter2},\phi} \\ I_{\text{Meter3},\phi} \\ I_{\text{Meter4},\phi} \\ I_{\text{Meter5},\phi} \\ I_{\text{Meter6},\phi} \\ I_{\text{Meter7},\phi} \end{bmatrix} \tag{1}$$

where $I_{\text{Meter1},\phi}, \ldots, I_{\text{Meter7},\phi}$ are the individual line currents of Meters 1–7 in this example. Since the power entering a node equals the power leaving that node, (1) can be applied for the P and Q for each phase. The matrix reflects the orientation and placement of the sensors and distribution system. If the system includes ring transformers that change the voltage, appropriate entries of the matrix can be scaled by the transformer turns ratio prior to applying KCL. A matrix can be built for both delta and wye configurations, provided that all sensors are measuring entirely either delta or wye wires. In the case of a system using a delta-wye or wye-delta transformer, each measured wye line current is related to a delta phase current, which is associated with two measured delta line currents, and all measurements must be converted to a uniform wye or delta set prior to applying KCL. The same wye-delta conversion will also be applied to each meter's P and Q measurements prior to summing. For four-wire wye systems, a neutral current sensor is unnecessary, as the neutral current in a wye system is only a result of phase current imbalances and does not change the power calculations. The neutral current can be calculated by summing the individual line currents.

III. Synchronization

DAQs collecting sensor measurements operate with an internal clock for sampling data. However, these clocks have limited accuracy, and the actual frequency of the clock may not precisely match a specified frequency. A time offset can appear between different DAQs. This causes drift in the KCL calculations that grow over time if left uncorrected. That is, if the meter sampling rates differ slightly, there also exists a time offset error that integrates over time. This offset must be continually corrected. This complicates applying (1) to recreate the ship total or switchboard powers. The DAQ used for testing, a LabJack UE9, has a rated maximum clock error

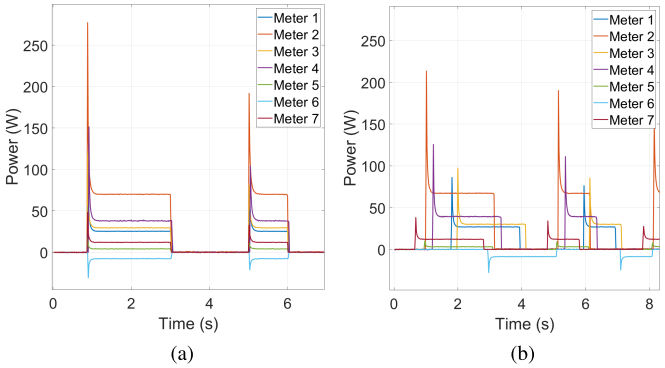

Fig. 3. Readings from all meters at beginning of data capture and after 24 h. (a) At start of data capture. (b) After 24 h.

of ±30 ppm [26]. Thus, the total error in one day can be up to 2.6 s. A test was run on the ring-bus setup in Fig. 1 with all power sources paralleled and the ring intact (and, thus, all seven meters reading a portion of the power stream), in which a resistive load on Switchboard 3 was cycled multiple times at the start of the test and again 24 h later. At the start of the test [see Fig. 3(a)], all the meters are aligned within a few samples of the 60-Hz sample points; however, after one day [see Fig. 3(b)], the meters have drifted, the furthest two being 2.3 s apart.

These time offsets between meters cause errors when computing KCL with (1), in particular, creating "artificial" transients (i.e., numerical artifacts due to time-alignment errors that could be misinterpreted as transient events) or distorted transients in the calculated switchboard power waveforms. Artificial and distorted transients are especially pronounced during load events, e.g., when a load turns on or off, and during changes in the generator configuration. If misaligned, a load event on a switchboard will be distorted and possibly unrecognizable in the KCL recreated power stream. The same load event also results in artificial transients in the other switchboards in the system with common meters. In one demonstration, for example, power is provided to the ring from two paralleled sources, Gen 1 and Shore, while a 250-W resistive load cycles on Switchboard 1, and a constant 90-W heater operates on Switchboard 2. Fig. 4(a) and (b) shows the reconstructed switchboard aggregate power without and with correction for the time shift, respectively. Without time alignment, both the on and off transients on Switchboard 1 are distorted. At the same time, the time misalignment causes power to be incorrectly attributed to Switchboard 2 and Switchboard 3 when KCL is performed. In contrast, when correctly aligned, Switchboards 2 and 3 show correct, constant steady-state values of 90 and 0 W, respectively, and Switchboard 1 shows clean on and off transients.

IV. Alignment Methods

An obvious solution is to use an external signal to precisely align the DAQ meter data. Wireless alignment signals, e.g., from GPS or a local substitute, may be difficult to transmit reliably on a ship, and a wired alignment signal may not be retrofittable to existing sensors. When an external time-alignment signal is not practical, the power system itself can be

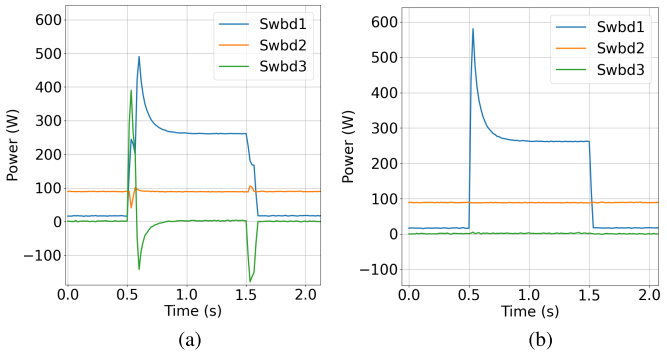

Fig. 4. Transient distortion and artificial transients in misaligned power streams. (a) Without time alignment. (b) With time alignment.

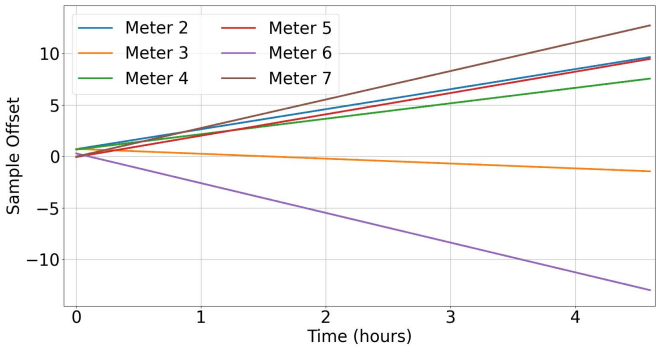

Fig. 5. DAQ sample offset drift continuously tracked with voltage zero-crossings.

used to align the data. Several different approaches can be used to "zero in" the alignment of the utility frequency cycles across the DAQs. Four methods are explored here. The first uses the voltage waveform zero-crossings to continuously track the time drifts. This method requires the initial time delay to be known. The other three methods can determine this delay, can also be used independently, and rerun periodically to realign DAQs as they drift. Methods are first explained individually but can be used together, as detailed in Section IV-E.

A. Zero-Crossing Delay Tracking

The voltage waveform on an ac utility is a classic source for a time reference; motorized wall clocks, for example, have been constructed for decades to take advantage of a reasonably controlled utility frequency for timekeeping. The zero-crossings of the utility voltage waveform can be used to continuously track and correct the DAQ time offset. Each positive zero-crossing is marked and timestamped using the Sinefit algorithm [25], but, because of individual DAQ inaccuracies, the timestamps themselves drift. Although each meter may have a slightly different sample rate, the zero-crossing event occurs consistently across all meters, making this an ideal "mile marker" for aligning the data. By simply maintaining a count of the zero-crossings, the time offsets between meters can be determined, and the power streams combined perfectly. Fig. 5 shows the calculated DAQ sample offset drift of each of the meters in the testbed power system relative to Meter 1. These drifts can be corrected by updating the timestamps.

The primary obstacle to using voltage zero-crossings for DAQ alignment arises from the ambiguity in the precise 60-Hz cycle being observed by a DAQ. We require an approach, analogous to a "home pulse" on a rotary encoder, which establishes the initial time delays between DAQs for correct relative counting of the different observed DAQ line cycles. There are many possible approaches for establishing the initial alignment for zero-crossings.

B. Voltage Correlation Alignment

Regardless of power flow through each meter, the voltage waveform is universally visible by all of the DAQs. Even a healthy electrical grid will not maintain a perfectly "stiff"

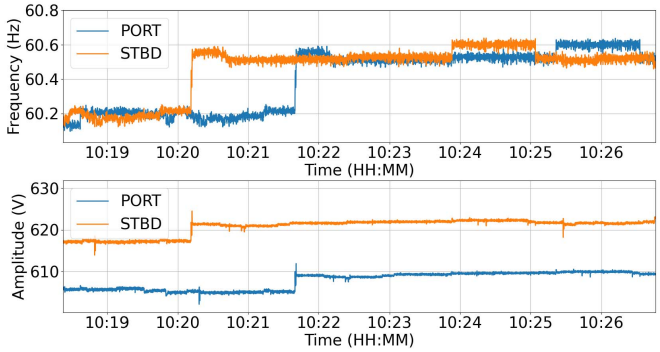

Fig. 6. Voltage frequency and amplitude from a USCG ship while underway.

voltage at all times, resulting in variations in both voltage amplitude and frequency. Microgrids are particularly susceptible to disturbances. These variations can be used as serendipitous events and patterns that provide alignment markers. The voltage frequency and amplitude are automatically calculated by the Sinefit algorithm [25], which uses successive four-parameter sine wave fitting to fit an observed voltage to the functional form

$$v[n] = A \cdot \sin\left(2\pi n \frac{f_0}{f_s} + \phi_0\right) + C \tag{2}$$

where A is the amplitude, f_0 is the line frequency, f_s is the sampling frequency, ϕ_0 is the phase angle, and C is the offset. For example, Fig. 6 shows the voltage frequency and amplitude data collected by two independent meters installed onboard a USCG ship, monitoring two separate subpanels (PORT and STBD). These data are taken while the ship is underway and the ship's grid is being powered by a ship service diesel generator (SSDG). Because of the limited generation capacity and finite inertia of a shipboard microgrid, there are frequently small fluctuations in supply frequency. A readily apparent time offset exists between the sample streams of these two meters.

The ring-bus demonstrator used for our laboratory testing draws power from a terrestrial grid, operating with a relatively stiff voltage waveform, but, even still, there are small voltage amplitude and frequency fluctuations as a result of changing loads on the grid. These "events" in voltage frequency and amplitude can be used to time-align the DAQ data. Fig. 7 shows the voltage frequency for two meters on the ring-bus

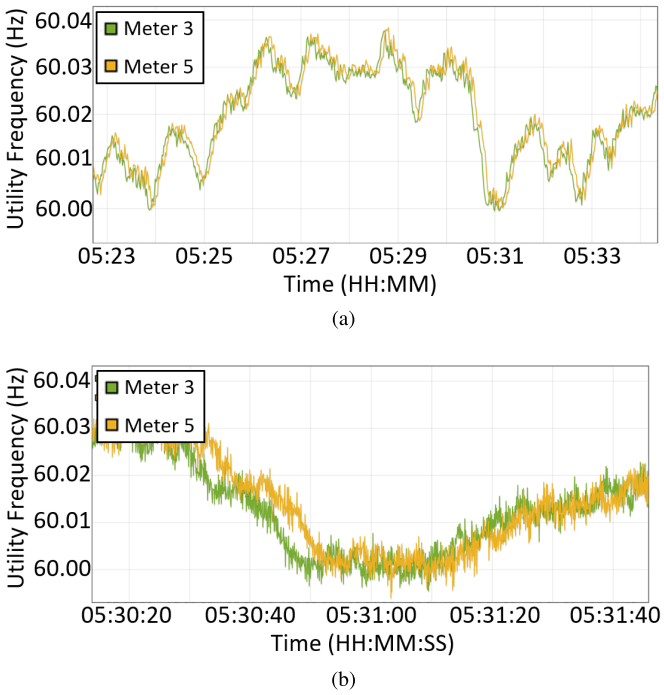

Fig. 7. Patterns visible in utility voltage frequency used for time alignment. (a) Frequency pattern over 10-min window. (b) Frequency pattern zoomed to 1-min window.

demonstrator; the pattern can be matched by cross correlation. The time window chosen for cross correlation needs to be large enough for these patterns to become visible. For a "stiffer" grid, the noise [as shown in Fig. 7(b)] in the frequency stream may dominate over smaller time windows and cause a loss of precision. Alignment of the ring-bus demonstrator using the grid was able to identify all meter delays to within one sample of the correct delay value. This precision may vary for different grids; thus, this method should be tested on the specific utility voltage waveform prior to use.

For a signal $s[n]$ observed by at least two DAQs, e.g., a utility voltage waveform, the measurement from the two meters $x[n]$ and $y[n]$ can be described as

$$\begin{aligned} x[n] &= s[n] + n_1[n] \\ y[n] &= s[n-D] + n_2[n], \quad 1 \le n \le N \end{aligned} \tag{3}$$

where D is the unknown delay, $n_1[n]$ and $n_2[n]$ are the noise of the two meters (assumed to be uncorrelated), and N is the number of samples. To time-align these meters, or a larger collection of DAQ meters, one stream is chosen as the base stream $x[n]$ and the delay D must be found for the remaining six meters with respect to $x[n]$. The estimated delay $\hat{D}$ is where the cross correlation of $x[n]$ and $y[n]$ is maximized [27]

$$\hat{D} = \max_{\tau} \; R_{xy}(\tau), \quad R_{xy}(\tau) = \sum_{n=1}^{N} x[n]y[n+\tau] \tag{4}$$

where τ is the time shift applied to the shifting meter $y[n]$ during the correlation process and ranges across the correlation window ($\tau = 1, \ldots, N$).

C. Adjacent Power Event Alignment

Observed load on and off events in the power stream can be used for time alignment. Transient events in the power stream are generally much larger and easier to detect than voltage variations. This approach requires identifying events in different meter power streams that are a result of the same physical event. Power flow is not uniformly or consistently distributed across all meters because different bus configurations shift the direction and amounts of power flowing around the ring bus. Thus, because it is not guaranteed that each meter is seeing all of the same events and because the power seen by each meter is not the same, the correlation-based method for voltage correlation alignment cannot be used here. Instead, an edge detector or change-of-mean detector is used to find the locations of on and off events in each power stream [28], and corresponding events between each meter are used to calculate the needed time-alignment shift. To determine corresponding events between meters, an assumption needs to be made about the maximum time shift that can occur between two meters. For example, if alignment is conducted immediately after the DAQs are activated, the maximum drift is bounded, e.g., to ten samples, or 1/6th of a second, based on the known DAQ hardware drift.

Using an edge detector to find the locations of all transient peaks in a given time window, a meter has a set of detected events $E = \{E_1, \ldots, E_M\}$ with corresponding sample indices $\{m_1, \ldots, m_M\}$, and a second meter has a set of detected events $F = \{F_1, \ldots, F_N\}$ with corresponding sample indices $\{n_1, \ldots, n_N\}$. The goal is the find the intersection of events, $E \cap F$. For each event in E with index i, the distance to the closest event in F is calculated

$$d_i = \min(m_i - n_j), \quad j = 0, \ldots, N. \tag{5}$$

The delay is estimated as the mean distance $\bar{d}$ using all $d_i \le B$, where B is the bounded maximum drift (ten samples in our testing)

$$\hat{D} = \text{mean}(d_i) \quad \forall \; i \text{ where } |d_i| \le B. \tag{6}$$

It is assumed that, when $d > B$, the event in E has no corresponding event in F, and the event is discarded. To minimize these discarded data, the meter with the maximum number of events provides the reference set of events E.

D. System Power Reconstruction

Alignment can also be performed by focusing on the end goal: no "artificial transients" in the calculated switchboard power stream. One meter is chosen as the reference meter, and data from the other meters surrounding that switchboard are shifted in time across a range of delay values τ. For each combination of delays, the estimated switchboard power stream is calculated by combining the meter power streams, using the relevant part of (1). Taking each recreated switchboard power stream P, a first-order difference filter is applied to generate an event stream

$$\Delta P[n] = P[n] - P[n-1]. \tag{7}$$

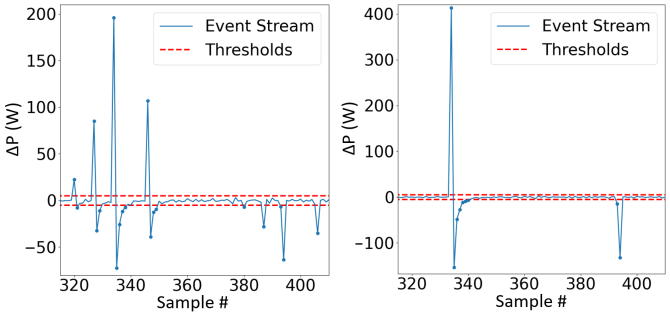

Fig. 8. Reconstructed switchboard event stream used for alignment by minimizing data points outside the threshold. (a) Incorrect delay values (τ); all four meter events misaligned. (b) Correct delay values (τ); all four meter events aligned.

If the meters are aligned, individual physical events seen by each meter will overlap in the reconstructed switchboard event stream, showing as a "single" event. However, if the meters are not aligned, individual physical events from each meter will be distanced from each other, appearing as "multiple" events in the switchboard event stream.

The four meters surrounding Switchboard 3 are used as an example here. A resistive load is cycled on and off, which results in a large positive peak at turn on followed by a large negative peak as inrush current fades and a negative peak at the turn-off event. Fig. 8(a) shows the event stream when the four meters of Switchboard 3 are not aligned. The four meters all see the same event, but summing the misaligned streams creates four separate peaks for the on-event and four separate peaks for the off-event in the event stream. In contrast, Fig. 8(b) shows that the time-aligned meters result in a single on-event and off-event. The event stream with the correct alignment will have the fewest event peaks. Choosing an appropriate threshold to filter out the noise (5 W in Fig. 8), the number of samples that fall outside this threshold is counted. The delay values yielding the minimum number of samples outside the threshold yield the correct alignment.

For example, for a three-meter system, the reference stream is given as $w[n]$, and streams $x[n]$ and $y[n]$ have unknown delays D_x and D_y. Then, C is calculated as the number of event stream samples outside the threshold γ for a range of delay values. The estimated delays $\hat{D}_x$ and $\hat{D}_y$ are the delay values (τ_x, τ_y) that minimize C

$$\hat{D}_x, \hat{D}_y = \min_{(\tau_x,\tau_y)} C, \quad C = \sum_n \begin{cases} 1, & |\Delta P_{(\tau_x,\tau_y)}[n]| > \gamma \\ 0, & |\Delta P_{(\tau_x,\tau_y)}[n]| \leq \gamma. \end{cases} \tag{8}$$

The values of C for a three-meter alignment over a 40-sample delay window is shown as a color plot in Fig. 9. Each axis represents the delay applied to each meter, shown as the number of samples one meter is shifted. The color plot makes clearly identifiable lines appear where two of the three meters align. In Fig. 9, A shows the minimum line where the x meter aligns with the w meter, B shows where the y meter aligns with the w meter, and C shows where the x meter aligns with the y meter. These three lines all cross at the absolute minimum point where all three meters align, which, in this

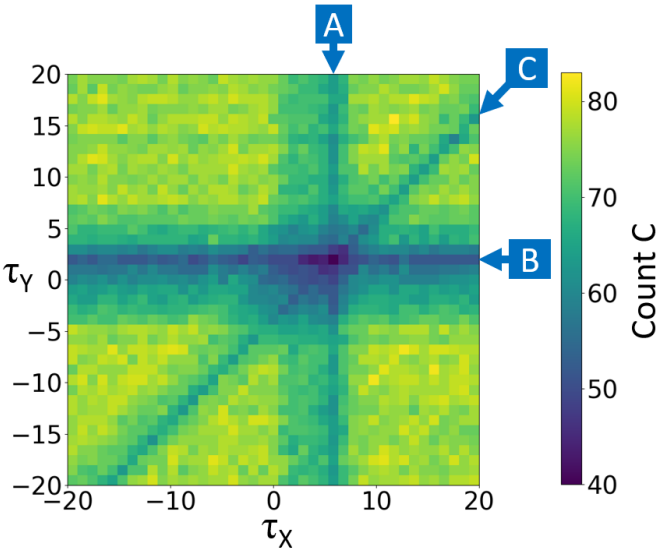

Fig. 9. Count of event stream samples outside threshold for two meters shifted by time delays (τ_x, τ_y). Minimum lines appear in the color plot where each meter aligns with the base meter (A and B) and with each other (C).

example, is the point $(\tau_x, \tau_y) = (6, 2)$. This tells us that the x-axis meter is offset by six samples, and the y-axis meter is offset by two samples.

This method is not limited to aligning three meters; additional meters simply add more dimensions. The largest number of meters aligned in our laboratory testing was four, as both Switchboard 3 current/power and total ship current/power calculations require up to four meters to reconstruct. The computation increases as larger windows and more meters are aligned as $O(m^{n-1})$, where m is the range of time delays tested and n is the number of meters being aligned. Distribution systems with more meters involved in reconstruction calculations will require drastically more computation. While this method will work for large offsets, it is preferable to use this method in smaller windows where meters are already known to be in close alignment to keep m low. Further research could optimize computations by searching for local minimums along several rows and columns, finding these partial alignment lines to point toward the complete alignment at the global minimum.

Once the meters surrounding each switchboard have been aligned with their neighbors, each switchboard can be aligned with the other switchboards by using common meters. The meters on the bus ties between switchboards are used in both switchboard alignment calculations and serve as intermediaries to calculating the total alignment of the system. Each bus tie meter reveals the delay of one switchboard relative to another switchboard, allowing all meters to be adjusted to align with one base meter. Alternatively, interswitchboard alignment can be found by performing this method using the meters of all online generators, reconstructing the total ship power instead of switchboard power. This will only align all three switchboards if all three generators are paralleled.

E. Method Choice

Each of these time-alignment methods has strengths and weaknesses when aligning several meters and can be combined

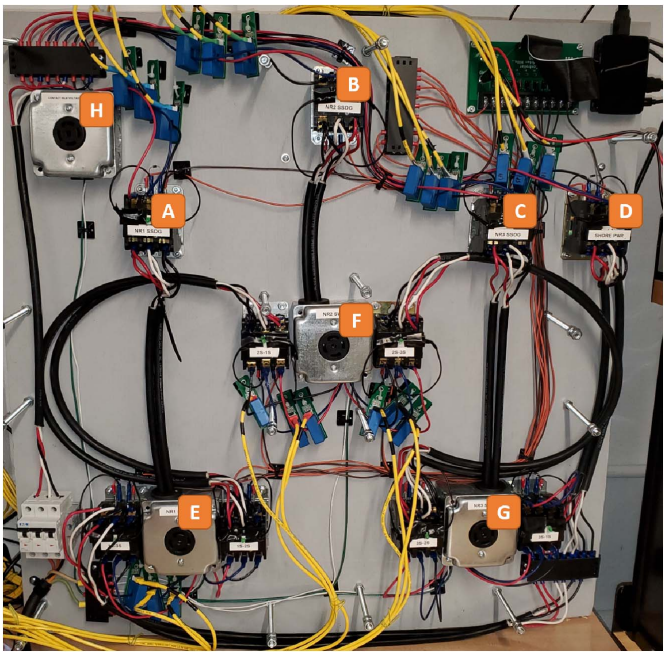

Fig. 10. Shipboard ring-bus demonstrator. Incoming power (H) splits into four power sources, (A) Gen 1, (B) Gen 2, (C) Gen 3, and (D) shore power, which feed three switchboards, (E) SWBD 1, (F) SWBD 2, and (G) SWBD 3. Current measurements are from the blue LA-55 current sensors.

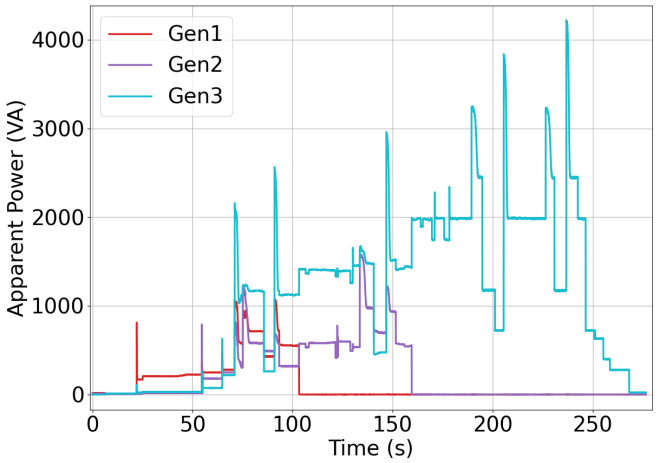

Fig. 11. Generator power streams during the test.

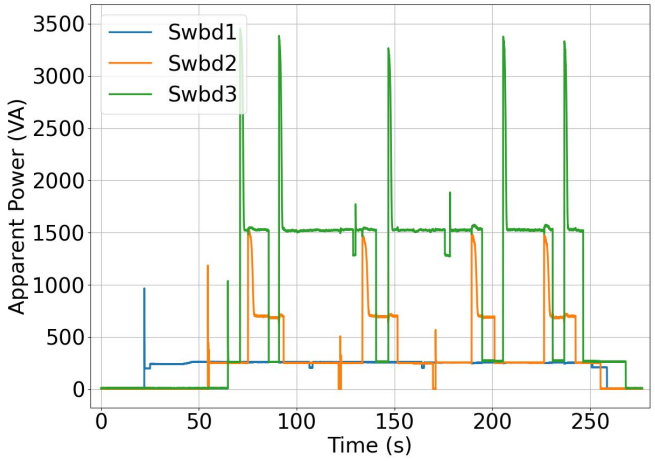

Fig. 12. Calculated switchboard power streams during the test.

to achieve greater certainty. The zero-crossing method can perfectly track the time-drift but relies on knowing the initial offset, which must be found through the other methods. The voltage correlation alignment method can be used to determine the offsets even in the absence of load transients. Voltage correlation alignment can also be used to quickly recover from large offsets and can be run periodically to maintain alignment throughout changing generator and bus configurations.

When load transient observations are available, the transient or power-based methods can be used. Adjacent power event (APE) alignment relies on having a known small offset; otherwise, physical events can no longer be correlated between different meters. When the offset is bounded, from either zero-crossing tracking or voltage correlation alignment, the power stream events can be used for finding the exact cycle-count integer offset. Another way to keep the offset small is to periodically restart the data capture. The system power reconstruction (SPR) can recover from large offsets, but computation time increases as the alignment window grows.

Particularly when used in combination, these methods provide strong data integrity for alignment. Prolonged periods without power transients reduce opportunities for employing some of the methods, but precise alignment of meters is only necessary when transients occur, as performing KCL using steady-state levels will not produce "artificial" transients.

V. Experimental Verification

To demonstrate the monitoring capability of switchboards fed by a ring bus, a ring-bus demonstrator was built and tested (see Fig. 10) following the USCG National Security Cutter schematic of Fig. 1. The test system emulates three ship service generators and a shore power connection, splitting incoming three-phase power into four different paths [29]. Relays serve as generator ties and breakers on the ring bus. A collection of L22-30 receptacles represent the switchboards, capable of providing power to load centers.

The time-correction methods were tested on the shipboard ring-bus demonstrator. For example, a 4-min segment of a test was run with a three-phase variable-speed motor operating on Switchboard 1, a 250-W resistive load and an axial fan on Switchboard 2 and a 250-W resistive load and a centrifugal fan on Switchboard 3. Various generator configurations were used to simulate different ship configurations. The various generator configurations are shown in Fig. 11. For a convenient visual display, the power is plotted as the total apparent power provided by each generator tie. DAQ time delays were calculated using the APE method, SPR method, and voltage correlation amplitude (VCA) and frequency (VCF) methods. Using Meter 1 as the reference stream, the relative line cycle offsets for Meters 2–7 are shown in Table I. All of these methods calculated the same offsets for all active meters. Shore power (Meter 4) was not paralleled during this test;

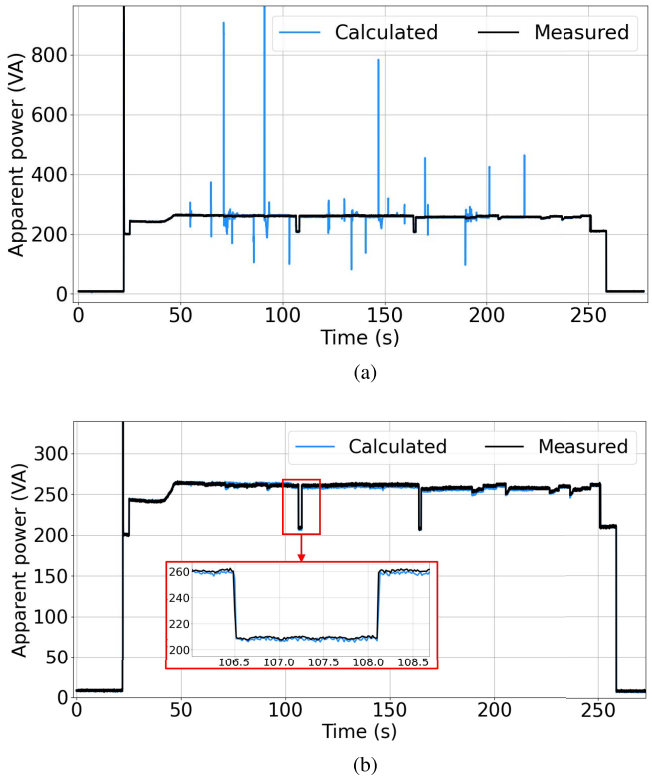

Fig. 13. Calculated and measured Switchboard 1 power during test (a) without time alignment and (b) with time alignment, with a zoomed-in view of a shorter window.

TABLE I
LINE CYCLE SAMPLE OFFSETS

	Meter2	Meter3	Meter4	Meter5	Meter6	Meter7
APE	2	0	N/A	4	-3	4
SPR	2	0	N/A	4	-3	4
VCF	2	0	2	4	-3	4
VCA	2	0	3	4	-3	4

thus, the methods that rely on load transients in the power stream (i.e., APE alignment and SPR) did not identify an offset value for Meter 4. However, the meter still recorded system voltage, allowing the offsets to be determined using voltage correlation alignment. Voltage amplitude and frequency alignment methods calculated two- and three-sample offsets, respectively, for Meter 4. Since Meter 4 observed no power flow and no load transients, the offset for Meter 4 does not affect switchboard reconstruction. The Meter 4 offset would be correctly computed, as for all other meters in the experiment, when load events are present.

Fig. 12 shows the calculated power for each of the three switchboards using the calculated sample offsets. For this test, an additional NILM meter was installed directly upstream of each switchboard so that the KCL-calculated power can be compared and cross-validated to directly measured switchboard power. Fig. 13(a) and (b) shows the calculated power for Switchboard 1 compared to the measured power without and with time alignment, respectively. For the nonaligned scenario in Fig. 13(a), there are many "artificial transients." These are a result of sample offsets between the meters causing power from Switchboards 2 and 3 to be incorrectly attributed to Switchboard 1 when KCL is performed. In contrast, the calculated waveform in Fig. 13(b) matches closely with the measured power. The root mean squared error (RMSE) calculation errors in apparent power for Switchboards 1–3 are 3.99, 10.10, and 25.37 VA, respectively. Without time alignment, the RMSEs for the three switchboards are 28.44, 32.74, and 37.37 VA, respectively.

VI. CONCLUSION

Perhaps, surprisingly given its familiarity, performing a practical KCL calculation is a challenge that requires precise time alignment of sensor readings to avoid both distorted and artificial transients. Experimental results from the ring-bus testbed demonstrate the feasibility and capability of a limited power monitoring system to track complex power distribution systems and loads without external time-alignment signals. Sources of potential time-alignment errors were identified and analyzed. The applicability of the time-alignment methods depends on several factors, such as if the initial time offset is known, the bounds of the time offset, the "stiffness" of the power system, and the occurrence of load transients. The evaluation showed that the combination of multiple time-alignment methods can provide greater data integrity. These time-alignment methods allow dual-use of existing grid sensors or the use of unmodified independent DAQs to feed data to a computer, which then calculates power flows around the grid and identifies loads via their on and off transients. The proposed monitoring system adds value to the management of energy resources and grid monitoring, collecting data for condition-based maintenance, electric plant load analysis (EPLA), fault detection, and failure response.

ACKNOWLEDGMENT

The authors gratefully acknowledge the support and dedication of the United States Coast Guard, in particular, the crew of USCGC Spencer.

REFERENCES

[1] J.-D. Park, J. Candelaria, L. Ma, and K. Dunn, "DC ring-bus microgrid fault protection and identification of fault location," *IEEE Trans. Power Del.*, vol. 28, no. 4, pp. 2574–2584, Oct. 2013.
[2] S. Mudaliyar and S. Mishra, "Coordinated voltage control of a grid connected ring DC microgrid with energy hub," *IEEE Trans. Smart Grid*, vol. 10, no. 2, pp. 1939–1948, Mar. 2019.
[3] M. Salehi, S. A. Taher, I. Sadeghkhani, and M. Shahidehpour, "A poverty severity index-based protection strategy for ring-bus low-voltage DC microgrids," *IEEE Trans. Smart Grid*, vol. 10, no. 6, pp. 6860–6869, Nov. 2019.
[4] B. Stevens, A. Dubey, and S. Santoso, "On improving reliability of shipboard power system," *IEEE Trans. Power Syst.*, vol. 30, no. 4, pp. 1905–1912, Jul. 2015.
[5] T. S. Ustun, C. Ozansoy, and A. Ustun, "Fault current coefficient and time delay assignment for microgrid protection system with central protection unit," *IEEE Trans. Power Syst.*, vol. 28, no. 2, pp. 598–606, May 2013.
[6] S. A. Saleh, "Signature-coordinated digital multirelay protection for microgrid systems," *IEEE Trans. Power Electron.*, vol. 29, no. 9, pp. 4614–4623, Sep. 2014.
[7] M. A. Haj-Ahmed and M. S. Illindala, "Investigation of protection schemes for flexible distribution of energy and storage resources in an industrial microgrid," *IEEE Trans. Ind. Appl.*, vol. 51, no. 3, pp. 2071–2080, May 2015.

[8] M. W. Rose and R. M. Cuzner, "Fault isolation and reconfiguration in a three-zone system," in *Proc. IEEE Electr. Ship Technol. Symp. (ESTS)*, Jun. 2015, pp. 409–414.
[9] S. R. Shaw, S. B. Leeb, L. K. Norford, and R. W. Cox, "Nonintrusive load monitoring and diagnostics in power systems," *IEEE Trans. Instrum. Meas.*, vol. 57, no. 7, pp. 1445–1454, Jul. 2008.
[10] A. Derviškadić, R. Razzaghi, Q. Walger, and M. Paolone, "The white rabbit time synchronization protocol for synchrophasor networks," *IEEE Trans. Smart Grid*, vol. 11, no. 1, pp. 726–738, Jan. 2020.
[11] A. Mahmood, M. I. Ashraf, M. Gidlund, J. Torsner, and J. Sachs, "Time synchronization in 5G wireless edge: Requirements and solutions for critical-MTC," *IEEE Commun. Mag.*, vol. 57, no. 12, pp. 45–51, Dec. 2019.
[12] M. Lévesque and D. Tipper, "A survey of clock synchronization over packet-switched networks," *IEEE Commun. Surveys Tuts.*, vol. 18, no. 4, pp. 2926–2947, 4th Quart., 2016.
[13] T.-C. Lin, H.-H. Wang, and C.-H. Liu, "Fault location for three-ended ring-topology power system using minimum GPS-based measurements and CVT/CT sensing," *IEEE Sensors J.*, vol. 21, no. 19, pp. 22019–22031, Oct. 2021.
[14] Y. Yuan, K. Dehghanpour, and Z. Wang, "Mitigating smart meter asynchrony error via multi-objective low rank matrix recovery," *IEEE Trans. Smart Grid*, vol. 12, no. 5, pp. 4308–4317, Sep. 2021.
[15] A. Alimardani, F. Therrien, D. Atanackovic, J. Jatskevich, and E. Vaahedi, "Distribution system state estimation based on nonsynchronized smart meters," *IEEE Trans. Smart Grid*, vol. 6, no. 6, pp. 2919–2928, Jun. 2015.
[16] X. Zeng, K. Liu, J. Ma, M. Chen, and M. Yu, "Reliability and delay trade-off analysis of unslotted IEEE 802.15.4 sensor network for shipboard environment," *IEEE Sensors J.*, vol. 21, no. 2, pp. 2400–2411, Jan. 2021.
[17] M. Chen, K. Liu, J. Ma, and C. Liu, "Spatio-temporal fingerprint localization for shipboard wireless sensor networks," *IEEE Sensors J.*, vol. 18, no. 24, pp. 10125–10133, Dec. 2018.
[18] I. Badran, M. T. Lazim, and M. Zeidan, "A general solution for ring-bus distribution systems reliability," in *Proc. 5th Int. Multi-Conf. Syst., Signals Devices*, Jul. 2008, pp. 1–4.
[19] G. Lipardi *et al.*, "Electric loads characterization in an aircraft carrier with ring-bus distribution system," in *Proc. Int. Conf. Electr. Syst. Aircr., Railway, Ship Propuls. Road Vehicles (ESARS)*, Mar. 2015, pp. 1–6.
[20] U. Orji *et al.*, "Load modeling for power system requirement and capability assessment," *IEEE Trans. Power Syst.*, vol. 30, no. 3, pp. 1415–1423, May 2015.
[21] *IEEE Recommended Practice for Electrical Installations on Shipboard–Design*, IEEE Standard 45.1-2017, 2017, pp. 1–198.
[22] W. C. Greene, "Evaluation of non-intrusive monitoring for condition based maintenance applications on U.S. Navy propulsion plantss," M.S. thesis, Massachusetts Inst. Technol., Cambridge, MA, USA, 2005.
[23] J. T. Leghorn, "Modeling for ship power system emulation," M.S. thesis, Massachusetts Inst. Technol., Cambridge, MA, USA, 2009.
[24] T. L. Hannon, "Integrated circuit breaker protection software," U.S. Patent 6 694 271 B1, Feb. 17, 2004.
[25] J. Paris, J. S. Donnal, Z. Remscrim, S. B. Leeb, and S. R. Shaw, "The sinefit spectral envelope preprocessor," *IEEE Sensors J.*, vol. 14, no. 12, pp. 4385–4394, Dec. 2014.
[26] *UE9 Datasheet*, Lakewood Corp., Lakewood, CO, USA, 2020.
[27] M. Azaria and D. Hertz, "Time delay estimation by generalized cross correlation methods," *IEEE Trans. Acoust., Speech, Signal Process.*, vol. ASSP-32, no. 2, pp. 280–285, Apr. 1984.
[28] A. Aboulian, J. S. Donnal, and S. B. Leeb, "Autonomous calibration of non-contact power monitors," *IEEE Sensors J.*, vol. 18, no. 13, pp. 5376–5385, Jul. 2018.
[29] R. C. Schaefer, "Art of generator synchronizing," *IEEE Trans. Ind. Appl.*, vol. 53, no. 1, pp. 751–757, Jan. 2017.

Brian T. Mills received the B.S. degree in naval architecture and marine engineering from the Webb Institute, Glen Cove, NY, USA, in 2016, and the M.S. degree in naval architecture and marine engineering from the Massachusetts Institute of Technology, Cambridge, MA, USA, in 2021.

He has served as a Student Engineer and an Assistant Engineer Officer of USCGC Stratton (WMSL 752). He is a Lieutenant with the United States Coast Guard. He is an Assistant Engineer Officer of USCGC Polar Star (WAGB 10).

Daisy H. Green (Graduate Student Member, IEEE) received the B.S. degree in electrical engineering from the University of Hawai'i at Mānoa, Honolulu, HI, USA, in 2015, and the M.S. degree in electrical engineering from the Massachusetts Institute of Technology, Cambridge, MA, USA, in 2018, where she is currently pursuing the Ph.D. degree.

John S. Donnal (Senior Member, IEEE) received the B.S. degree from Princeton University, Princeton, NJ, USA, in 2007, and the M.S. and Ph.D. degrees from the Massachusetts Institute of Technology, Cambridge, MA, USA, in 2013 and 2016, respectively, all in electrical engineering.

He is currently working as a Faculty Member with the U.S. Naval Academy in Weapons, Robotics, and Control Engineering. His research interests include nonintrusive load monitoring synthesis, energy harvesting, and communications systems.

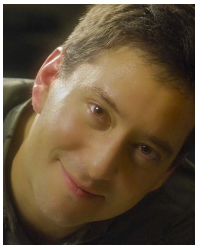

Steven B. Leeb (Fellow, IEEE) received the Ph.D. degree from the Massachusetts Institute of Technology (MIT), Cambridge, MA, USA, in 1993.

Since 1993, he has been a member of the MIT Faculty, Department of Electrical Engineering and Computer Science, MIT. He also holds a joint appointment with the Department of Mechanical Engineering, MIT. He is concerned with the development of signal processing algorithms for energy and real-time control applications.